future internet

MDPI

Article

Precoding for RIS-Assisted Multi-User MIMO-DQSM Transmission Systems

Francisco R. Castillo-Soria [1,†], J. Alberto Del Puerto-Flores [2,*,†], Cesar A. Azurdia-Meza [3,†], Vinoth Babu Kumaravelu [4,†], Jorge Simón [5,†] and Carlos A. Gutierrez [1,†]

1 Department of Telecommunications, Faculty of Science, Universidad Autonoma de San Luis Potosi, San Luis Potosi 78210, Mexico; ruben.soria@uaslp.mx (F.R.C.-S.); cagutierrez@ieee.org (C.A.G.)
2 Facultad de Ingeniería, Universidad Panamericana, Álvaro del Portillo 49, Zapopan 45010, Mexico
3 Department of Electrical Engineering, Universidad de Chile, Santiago 8370451, Chile; cazurdia@ing.uchile.cl
4 Department of Communication Engineering, School of Electronics Engineering, Vellore Institute of Technology, Vellore 632014, India; vinothbab@gmail.com
5 Catedras CONACYT, Unidad Academica de Ingenieria Electrica, Universidad Autonoma de Zacatecas, Zacatecas 98000, Mexico; jsimonro@conacyt.mx
* Correspondence: jpuerto@up.edu.mx
† These authors contributed equally to this work.

Abstract: This paper presents two precoding techniques for a reconfigurable intelligent surface (RIS)-assisted multi-user (MU) multiple-input multiple-output (MIMO) double quadrature spatial modulation (DQSM) downlink transmission system. Instead of being applied at the remote RIS, the phase shift vector is applied at the base station (BS) by using a double precoding stage. Results show that the proposed RIS-MU-MIMO-DQSM system has gains of up to 17 dB in terms of bit error rate (BER) and a reduction in detection complexity of 51% when compared with the conventional MU-MIMO system based on quadrature amplitude modulation (QAM). Compared with a similar system based on amplify and forward (AF) relay-assisted technique, the proposed system has a gain of up to 18 dB in terms of BER under the same conditions and parameters.

Keywords: precoding; RIS; double-QSM; MIMO; multi-user detection

Citation: Castillo-Soria, F.R.; Del Puerto-Flores, J.A.; Azurdia-Meza, C.A.; Babu Kumaravelu, V.; Simón, J.; Gutierrez, C.A. Precoding for RIS-Assisted Multi-User MIMO-DQSM Transmission Systems. *Future Internet* **2023**, *15*, 299. https://doi.org/10.3390/fi15090299

Academic Editors: Sachin Sharma, Nouman Ashraf and Claude Chaudet

Received: 16 July 2023
Revised: 28 July 2023
Accepted: 21 August 2023
Published: 2 September 2023

1. Introduction

Massive multiple-input multiple-output (MIMO) in combination with leading-edge technologies, methodologies, and architectures are poised to be a cornerstone technology for the next-generation wireless systems and networks. The capabilities and performance of future massive MIMO systems will be enhanced through the incorporation of reconfigurable intelligent surface (RIS), artificial intelligence (AI), Terahertz (THz) communications, and cell-free architectures [1]. In particular, RIS-assisted systems have been recently proposed as one of the key enabling technologies for beyond 5G/6G wireless communication networks to support a massive number of users at a high data rate, low latency, and secure transmissions with both spectral and energy efficiency [2–4]. A RIS is a surface of electromagnetic metamaterial that can control the phase, amplitude, frequency, and/or polarisation of the impinging signals in a nearly passive way without the need for radio-frequency (RF) operations [5,6]. For example, the RIS can be designed to coherently combine the signals in the reception. In this way, the RIS changes the destructive effect of the multipath fading channel into a controllable channel that exploits diversity gains to improve the performance of the system. As a result, the overall energy of the transmitted signals can be used more efficiently. Since the RIS does not amplify the signals, RF chains are not required and thermal noise is not added during reflections [7–9]. RIS-assisted systems can be further improved if intelligent omni-surface (IOS) are considered. IOS-based systems can achieve full-dimensional wireless communications by enabling the simultaneous reflection and

refraction of the surface, and thus users on both sides can be served [10]. Due to the system's complexity, the analysis is typically limited to single-antenna users and single Tx antenna systems [11].

In particular, some frameworks for the implementation of RIS-assisted multi-user (MU) downlink transmission systems have been recently proposed [12–16]. In these previous works, the design of the system is mainly focused on the optimization problem for the joint design of the beamforming matrix at the base station (BS) and the phase shift vector at the RIS. As a result, the design of the system leads to a non-convex optimization problem. When full MIMO systems are considered, the main drawback of the systems is the high complexity of the optimization algorithms which require intensive signal processing and frequent actualization of the channel state information (CSI) at the RIS. This approach can be a challenge mainly for the future massive MIMO (mMIMO) systems [2]. Additionally, the practical implementation of RIS-assisted MU-MIMO systems can be complicated considering that the RIS could be located at remote places. Recently, linear precoding has been used to simplify the complexity of RIS-assisted transmission systems [17]. The precoding strategy can be effective to reduce the overloaded RIS while allowing to eliminate interference [18].

Inspired by the above, this paper presents two precoding strategies for the transmission of double quadrature spatial 2 modulation (DQSM) signals in a RIS-assisted MU-MIMO scenario. In the first strategy, the proposed system uses two precoding stages at the BS. The first precoding stage applies the optimal amplitudes and phases required to pre-cancel the MU interference (MUI) in the second hop (from the RIS to the users). The second precoder is designed to pre-cancel the interference in the first hop (from the BS to the RIS). This strategy guarantees that the RIS reflects the signals with the appropriate amplitude and phase, producing an interference-free signal at the receivers. A second strategy, that combines the two precoding blocks in just one, is also presented. The two proposed strategies are evaluated considering a correlated fading channel and two different configurations. The overall system performance is improved by incorporating a DQSM transmission scheme [19]. Spatial modulation (SM) not only improves the bit error rate (BER) performance, but also reduces the detection complexity of the proposed system [20,21]. Results show that the proposed system generates the desired interference-free signals at the mobile station (MS) with diversity gains. Moreover, the proposed system clearly outperforms a conventional MU-MIMO system based on spatial multiplexing (SMux) and quadrature amplitude modulation (QAM) [22], and the amplify and forward (AF) relay-assisted MU-DQSM system [23] used as references. To the best of the author's knowledge, the proposed system has not been addressed in previous works.

The remainder of this work is organized as follows. In Section 2, the system model of the RIS-MU-DQSM system is introduced. In Section 3, the channel model is presented. Section 4, discusses the interference cancellation of the system, whereas Section 5 deals with the optimal detection. Section 6 shows the results of the BER performance and the detection complexity of the proposed systems. Also, this section discusses the obtained results. Finally, conclusions are provided in Section 7.

Notation: Uppercase boldface letters denote matrices whereas lowercase boldface letters denote vectors. The transpose, Hermitian transpose, complex conjugate, and Frobenius norm of $\mathbf{A}$ are denoted by $\mathbf{A}^T$, $\mathbf{A}^H$, $\mathbf{A}^*$, and $\|\mathbf{A}\|_F$, respectively. The statistical expectation is represented by $E[\cdot]$, $\mathbf{0}$ denotes an all-zero matrix (or vector) whose dimensions are specified according to the context. Finally, $\mathcal{CN}(0, \sigma^2)$ is used to represent the circularly symmetric complex Gaussian distribution with mean zero and variance σ^2.

2. System Model

The RIS-MU-DQSM system model is presented in Figure 1. We assume that there is not a direct link between the transmitter (Tx) and receivers (Rx), which can be due to unfavorable propagation conditions or blockings by obstacles [24,25]. All communication passes through the RIS. The BS is equipped with N_t Tx antennas, while the desti-

nation is composed of K users or MS, each one equipped with N_r Rx antennas. The RIS uses N_s reflective surfaces. Thus, the end-to-end configuration can be considered as a $(K \times N_r) \times N_s \times N_t$ RIS-assisted MU-MIMO-DQSM transmission system, hereinafter referred to as RIS-MU-DQSM.

The channel matrix between the BS and the RIS is defined as $\mathbf{G} \in \mathbb{C}^{N_s \times N_t}$. The channel matrix between the RIS and the k-th MS is defined as $\mathbf{H}_k \in \mathbb{C}^{N_r \times N_s}$. The channel model is defined for two scenarios. First, a quasi-static Rayleigh fading channel is considered where its elements are assumed to be independent and identically distributed (i.i.d.) complex Gaussian random variables with mean zero and variance one, $\mathcal{CN}(0,1)$. Additionally, a more realistic channel model where the spatial correlation between the RIS mirrors is considered. We assume that perfect CSI is available at the BS and all MS or users. It is worth noting that obtaining CSI can be a challenging task [26]. As has been proposed in previous works, this task can be carried out using control links between the BS and the users when the line-of-sight (LoS) path is absent in this channel [27,28]. However, the design of CSI dissemination strategies is beyond the scope of this work.

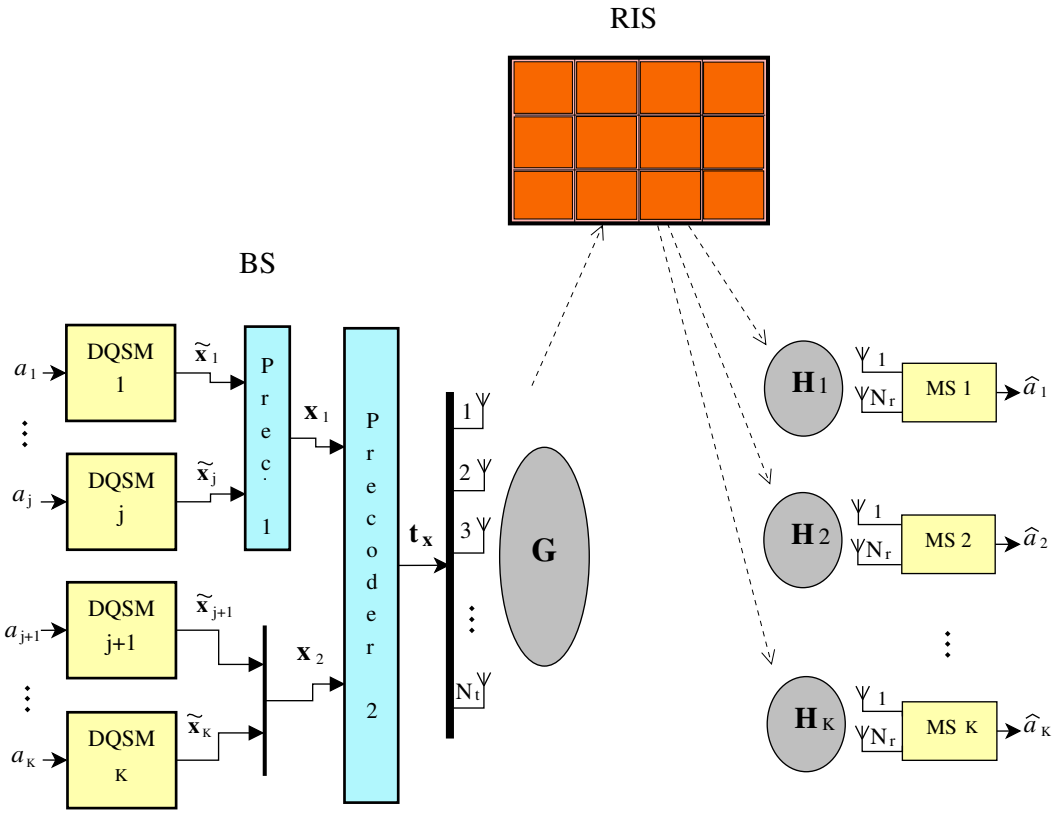

Figure 1. RIS-Assisted MU-DQSM system model.

2.1. Transmission

In order to generate the DQSM signal, the sequence of input bits $\mathbf{a}_k = \{d_n\}_{n=1}^{m}$, with $d_n \in \{0,1\}$ is split in two flows. Each data flow is composed of a sequence $\mathbf{b}_k = \{d_n\}_{n=1}^{m/2}, k = \{1,2\}$, which is fed into a quadrature spatial modulation (QSM) block. Figure 2 shows the DQSM modulation block used for the proposed scheme. The QSM signals are denoted by $\mathbf{x}'_i \in \mathbb{C}^{L\times 1}, i = \{1,2\}$, with components $x'_l \in \{0, s_\Re, s_\Im\}$ where $s_\Re$ and $s_\Im$ represent the real and the imaginary parts of the quadrature amplitude modulation of M-th order (M-QAM) symbol s, respectively. The output vector of the i-th QSM block $\mathbf{x}'_i$ is defined as

$$\mathbf{x}'_i = (x'_1, x'_2, \ldots, x'_L)^T, i = \{1,2\}, \quad (1)$$

where the index in $\tilde{x'}_i$ denotes the transmitted signal in the k-th position. In order to generate the QSM vector $\mathbf{x'}_i$, the input bit sequence is divided into three streams. One

stream is used to modulate a M-QAM signal and the other two streams (spatial bits) are used to modulate the position in the QSM output vector. For an input bit sequence of length $m_{QSM} = m_{DQSM}/2$, the first $\log_2(M)$ bits modulate a M-QAM symbol, the remaining $2\log_2(L) = m_{QSM} - \log_2(M)$ bits are divided into two streams with $\log_2(L)$ spatial bits each. These spatial bits modulate the position of the M-QAM symbol in the output vector $\mathbf{x'}_i \in \mathbb{C}^{L\times 1}$ using an SM block as follows: the real part of the M-QAM symbol is assigned to a specific position in the output vector, while the remaining $L-1$ positions are set to zero. The imaginary part of the M-QAM symbol is assigned to another or even the same position in the output vector. Finally, these two signals are combined to obtain the QSM output vector $\mathbf{x'}_i$ [29]. The number of bits that can be transmitted using QSM is $m_{QSM} = log_2(M) + 2log_2(L)$, The two QSM signals $\mathbf{x}'_1$ and $\mathbf{x}'_2$ are then weighted by the factors B_1 and B_2, which guarantee the maximal Euclidean distance between symbols. These two signals are combined to generate the DQSM output vector $\tilde{\mathbf{x}}_k$ intended for the k-th user as [19]

$$\tilde{\mathbf{x}}_k = B_1\mathbf{x}'_1 + B_2\mathbf{x}'_2. \tag{2}$$

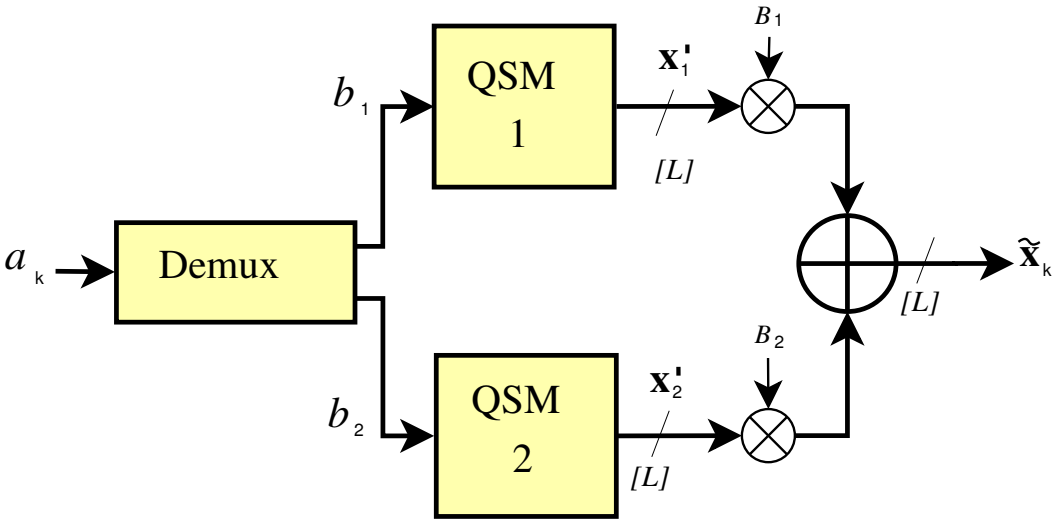

Figure 2. DQSM modulation block.

The output vector of the k-th DQSM block $\tilde{\mathbf{x}}_k \in \mathcal{A}$ can be written as

$$\tilde{\mathbf{x}}_k = (\tilde{x}_1, \tilde{x}_2, \ldots, \tilde{x}_L)^T, \tag{3}$$

where the index in $\tilde{x}_l$ denotes the transmitted signal in the l-th position. The complete transmission block for K users in the system before precoding is composed as

$$[\tilde{\mathbf{x}}_1, \tilde{\mathbf{x}}_2, \ldots, \tilde{\mathbf{x}}_j, \tilde{\mathbf{x}}_{j+1}, \ldots, \tilde{\mathbf{x}}_K]. \tag{4}$$

where the first j users are the users under multiuser interference (MUI). The other $K-j$ users are the users free from MUI. The number of bits that can be transmitted to each user using DQSM is

$$m_{DQSM} = 2(log_2(M) + 2log_2(L)). \tag{5}$$

DQSM is mainly used because it has good BER performance and low detection complexity [19].

As shown in Figure 1, the precoder is composed of two stages. Users under MUI are first taken to Precoder 1. The Precoder 1 is intended to pre-cancel the MUI in the second hop (from the RIS to the MS). The output of Precoder 1 is the vector $\mathbf{x}_1$ defined as

$$\mathbf{x}_1 = \sum_{k=1}^{j} \mathbf{W}_k\tilde{\mathbf{x}}_k = (x_1, x_2, \ldots, x_{N'_s})^T. \tag{6}$$

In Precoder 1, the vectors $\tilde{\mathbf{x}}_k$ are precoded by the matrices $\mathbf{W}_k \in \mathbb{C}^{N_s' \times N_r'}$, where $N_s' \leq N_s$ is the number of reflecting mirrors intended for users under MUI and $N_r' \leq N_r$ is the number of receive antennas in this subset. Users who are not under MUI, are concatenated in the vector $\mathbf{x}_2$ and then are taken to Precoder 2. The input vector to Precoder 2 is

$$\mathbf{x} = (\mathbf{x}_1^T, \mathbf{x}_2^T)^T. \tag{7}$$

The Precoder 2 is designed to pre-cancel the interference in the first hop (from the BS to the RIS). It guarantees that the signals with appropriate phases and amplitudes are reflected by the RIS. The output signal $\mathbf{t_x} \in \mathbb{C}^{N_t \times 1}$ of Precoder 2 can be written as

$$\mathbf{t_x} = \mathbf{F}\mathbf{x}, \tag{8}$$

where $\mathbf{F} \in \mathbb{C}^{N_t \times N_s}$ is a precoding matrix. Table 1 shows the first 16 out of 256 DQSM signals.

Table 1. DQSM signal generation example for $M = 4$, $L = 2$.

Input Bits, a_k b_1 b_2	**QSM 1** x'_1	**QSM 2** x'_2	**Output Signal DQSM**
0000 0000	$1+j, 0$	$1+j, 0$	$1.5+1.5j, 0$
0000 0001	$1+j, 0$	$-1+j, 0$	$0.5+1.5j, 0$
0000 0010	$1+j, 0$	$1-j, 0$	$1.5+0.5j, 0$
0000 0011	$1+j, 0$	$-1-j, 0$	$0.5+0.5j, 0$
0000 0100	$1+j, 0$	$1, j$	$1.5+j, 0.5j$
0000 0101	$1+j, 0$	$-1, j$	$0.5+j, 0.5j$
0000 0110	$1+j, 0$	$1, -j$	$1.5+j, -0.5j$
0000 0111	$1+j, 0$	$-1, -j$	$0.5+j, -0.5j$
0000 1000	$1+j, 0$	$j, 1$	$1+1.5j, 0.5$
0000 1001	$1+j, 0$	$j, -1$	$1+1.5j, -0.5$
0000 1010	$1+j, 0$	$-j, 1$	$1+0.5j, 0.5$
0000 1011	$1+j, 0$	$-j, -1$	$1+0.5j, -0.5$
0000 1100	$1+j, 0$	$0, 1+j$	$1+j, 0.5+0.5j$
0000 1101	$1+j, 0$	$0, -1+j$	$1+j, -0.5+0.5j$
0000 1110	$1+j, 0$	$0, 1-j$	$1+j, 0.5-0.5j$
0000 1111	$1+j, 0$	$0, -1-j$	$1+j, -0.5-0.5j$

2.2. Reception

The impinging signals at the RIS are defined as

$$\mathbf{r} \triangleq \sqrt{1/\alpha}\mathbf{G}\mathbf{t_x}, \tag{9}$$

where $\mathbf{t_x} \in \mathbb{C}^{N_t \times 1}$ is the signal vector transmitted by the BS and $\sqrt{1/\alpha}$ is an attenuation factor. These signals are reflected by the RIS without adding noise. Then, the received signal by the k-th user in the destination is given by

$$\mathbf{y}_k = \sqrt{\gamma}_k \mathbf{H}_k \mathbf{\Theta} \mathbf{G} \mathbf{t_x} + \mathbf{n}_k, \tag{10}$$

where $\mathbf{\Theta}$ is the phase shift matrix, defined as $\mathbf{\Theta} = \text{diag}(e^{j\theta_1}, e^{j\theta_2}, \ldots, e^{j\theta_{N_S}})$. Here, $e^{j\theta_i}$ denotes the phase shift of the i-th reflecting element at the RIS and $\mathbf{n}_k \in \mathbb{C}^{N_r \times 1}$ stands for the noise. The noise samples are assumed to be independent and identically distributed (i.i.d) with $\mathcal{CN}(0, \sigma^2)$. $\sqrt{\gamma}_k$ is the signal-to-noise ratio (SNR) at the destination. Instead of applying the phase shifts vector at the RIS, in this work, the signals with optimal phases and amplitudes required at the RIS are evaluated and implemented in the BS. Since only precoding is used, the phases in the RIS can be considered arbitrary or fixed. In this paper, the RIS is considered as "blind" with $\mathbf{\Theta} = \mathbf{I}$.

3. Channel Model

For the channel model, we consider a flat fading Rayleigh channel where both the BS and the RIS are affected by spatial correlation. Note that mirrors can be optimally selected for a particular user in order to minimize the spatial correlation in the RIS. However, this approach is beyond the scope of this work. The proper operation of the system requires that each user could be illuminated by a subgroup of mirrors of at least $N_s' = N_r$. If $N_s' > N_r$, the receptor can take advantage of diversity gains. In order to evaluate the effects of the spatially correlated fading channel, the following Kronecker model is considered [30]:

$$\mathbf{G} = \mathbf{R}_\mathbf{r}^{1/2}\mathbf{H}^w\mathbf{R}_\mathbf{t}^{1/2}, \tag{11}$$

where the elements of the matrix $\mathbf{H}^w$ are assumed to be independent and i.i.d. complex Gaussian random variables with mean zero and variance one, $\mathcal{CN}(0,1)$. The matrices $\mathbf{R}_r$ and $\mathbf{R}_t$ are the receive and transmit correlation matrices, respectively. The correlation matrices are defined using the exponential model as

$$\mathbf{R}_t = \begin{bmatrix} 1 & \rho_t^* & \rho_t^{2*} & \cdots & \rho_t^{(N_t-1)*} \\ \rho_t & 1 & \rho_t^* & & \rho_t^{(N_t-2)*} \\ \rho_t^2 & \rho_t & 1 & & \vdots \\ \vdots & & & \ddots & \\ \rho_t^{(N_t-1)} & \rho_t^{(N_t-2)} & & & 1 \end{bmatrix}, \tag{12}$$

$$\mathbf{R}_r = \begin{bmatrix} 1 & \rho_r^* & \rho_r^{2*} & \cdots & \rho_r^{(N_r-1)*} \\ \rho_r & 1 & \rho_r^* & & \rho_r^{(N_r-2)*} \\ \rho_r^2 & \rho_r & 1 & & \vdots \\ \vdots & & & \ddots & \\ \rho_r^{(N_r-1)} & \rho_r^{(N_r-2)} & & & 1 \end{bmatrix}, \tag{13}$$

where ρ_t and ρ_r are the correlation coefficients between adjacent antennas at the transmitter and the receiver sides, respectively. In this work, we consider a correlated channel in the transmission and the reception side of the first hop for all evaluated systems.

4. Interference Cancellation

As shown in Figure 3, MUI can be present in the system whenever two or more users are under the same beams. However, other users who are far away are free from interference. Since the RIS does not has the capacity to cancel the interference produced in the first hop, a zero-forcing (ZF) technique is adequate for this precoding stage [31,32]. Therefore, the complete transmission block is precoded by using ZF. Additionally, for that user under MUI, a block diagonalization (BD) precoding technique is first used [33]. The BD technique is implemented to design the phase and the amplitude of the reflected signals in the RIS. Note that the ZF technique cancels the channel. However, CSI in the second hop is used to transmit the spatial modulated signals, assuring that the complete information can be retrieved by the users at the destination. For the implementation of the system, two strategies are used. Strategy I is used when some users are under MUI, as shown in Figure 3. Strategy II can be used when all users are under MUI or all users can see the entire RIS.

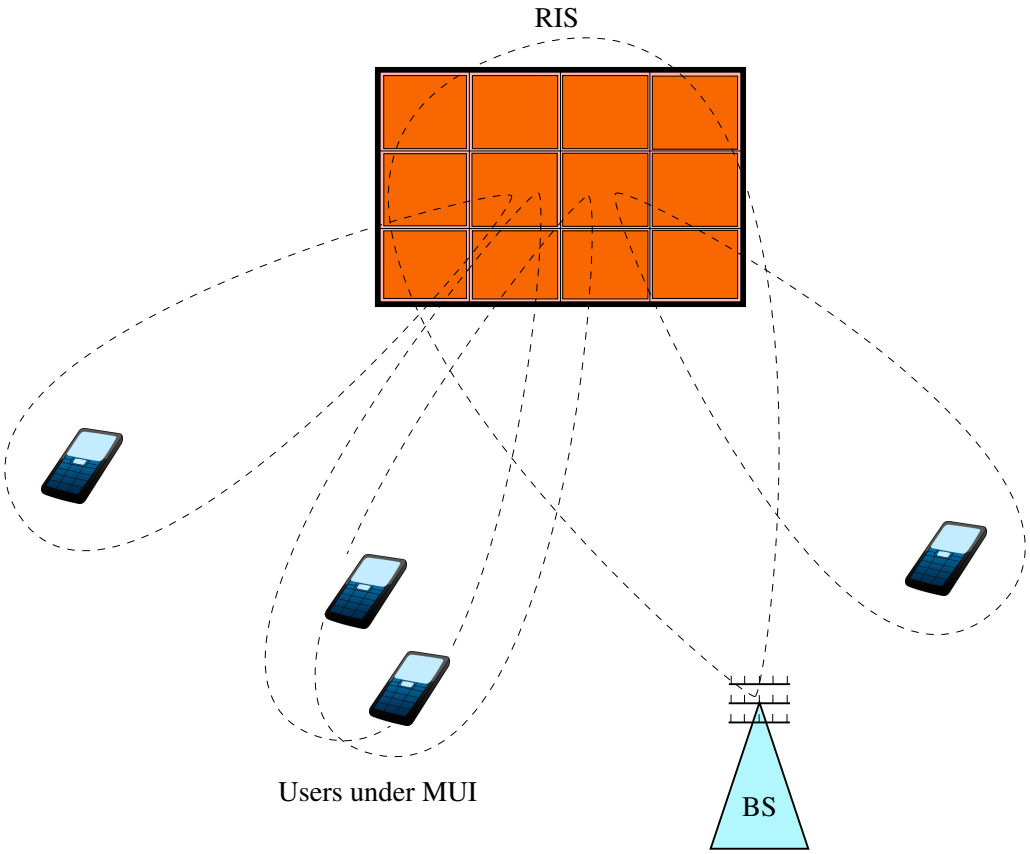

Figure 3. Users under MUI are illuminated by two or more beams.

4.1. Strategy I. ZF-BD Precoding

In this strategy, firstly a BD technique is used in Precoder 1 at the BS to generate the signals with appropriate phases required by the RIS in order to cancel the interference in the second hop. Then, a ZF technique is used in Precoder 2 to pre-cancel the interference in the first hop. Figure 4 shows a block diagram of Strategy I.

Strategy I can be used when some users are MUI-free. Let us consider a ZF precoding in Precoder 2. The precoding matrix is defined as $\mathbf{F} = \mathbf{G}^{+}$. Then, the output can be written as [32]

$$\mathbf{t_x} = \mathbf{Fx}, \tag{14}$$

where $\mathbf{G}^{+}$ represent the inverse of the channel matrix $\mathbf{G}$. Substituting (14) in (10) and considering the blind RIS, we obtain

$$\mathbf{y}_k = \sqrt{\gamma_k}\mathbf{H}_k\mathbf{x} + \mathbf{n}_k. \tag{15}$$

Equation (15) represents the signals received by all users. For users that are free from MUI, the received signal is

$$\mathbf{y}'_k = \sqrt{\gamma_k}\mathbf{H}_k\mathbf{x}_2 + \mathbf{n}_k. \tag{16}$$

Since $\mathbf{y}'_k$ is free from MUI, only Precoder 2 is used to precancel the interference. For users affected by MUI, and substituting (6) in (15), the received signal $\mathbf{y}_k$ by the k-th user is

$$\mathbf{y}_k = \sqrt{\gamma_k}\mathbf{H}_k \sum_{k=1}^{j} \mathbf{W}_k\tilde{\mathbf{x}}_1^k + \mathbf{n}_k, \tag{17}$$

where j is the number of users under MUI. Equation (17) can be rewritten as

$$\mathbf{y}_k = \sqrt{\gamma}_k \mathbf{H}_k \mathbf{W}_k \tilde{\mathbf{x}}_1^k + \sqrt{\gamma}_k \mathbf{H}_k \sum_{i=1, i\neq k}^{j} \mathbf{W}_i \tilde{\mathbf{x}}_1^i + \mathbf{n}_k. \tag{18}$$

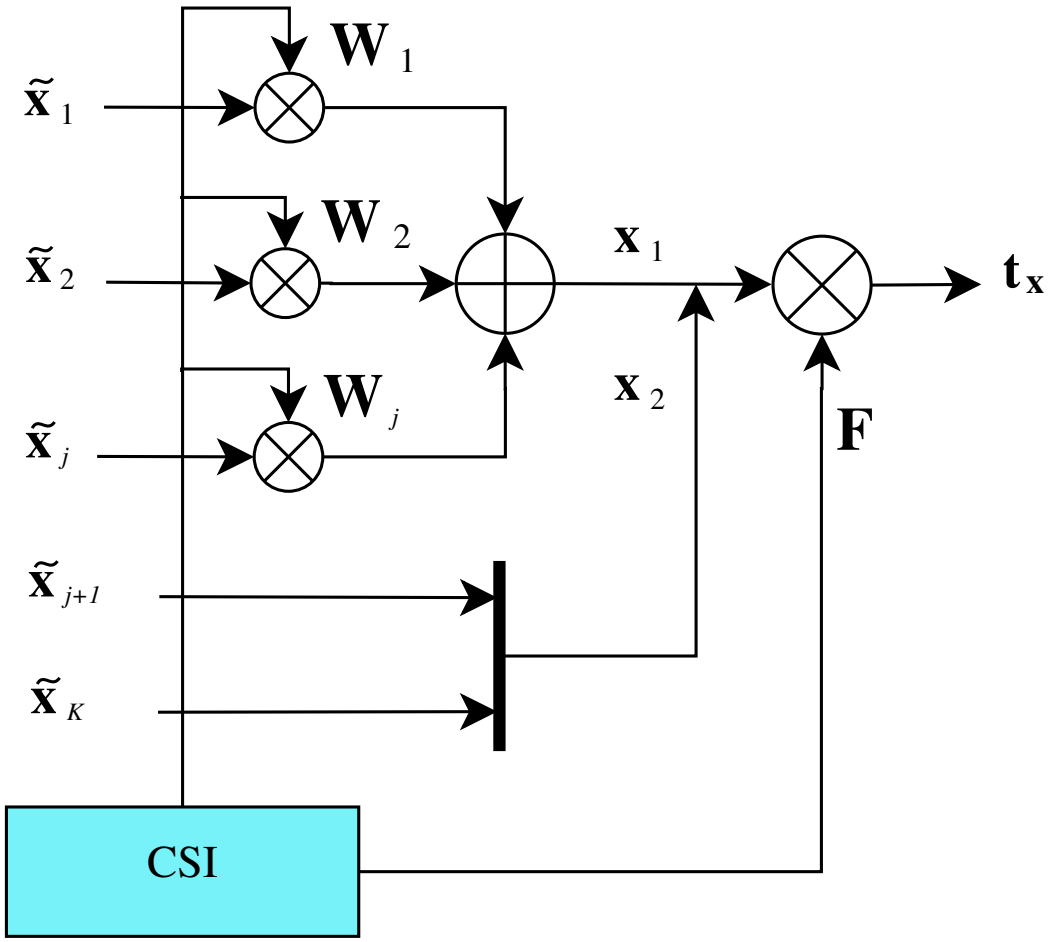

Figure 4. Strategy I (ZF-BD precoding technique).

The first term in (18) is the signal intended for the k-th user, the second term is the interference produced by the other users in the system, whereas the third term is noise. The mathematical model of the complete system can be represented as

$$\begin{bmatrix} \mathbf{y}_1 \\ \mathbf{y}_2 \\ \vdots \\ \mathbf{y}_j \end{bmatrix} = \begin{bmatrix} \mathbf{H}_1 & \mathbf{H}_1 & \cdots & \mathbf{H}_1 \\ \mathbf{H}_2 & \mathbf{H}_2 & \cdots & \mathbf{H}_2 \\ \vdots & & \ddots & \vdots \\ \mathbf{H}_j & \mathbf{H}_j & \cdots & \mathbf{H}_j \end{bmatrix} \begin{bmatrix} \mathbf{W}_1 \tilde{\mathbf{x}}_1^1 \\ \mathbf{W}_2 \tilde{\mathbf{x}}_1^2 \\ \vdots \\ \mathbf{W}_j \tilde{\mathbf{x}}_1^j \end{bmatrix} + \begin{bmatrix} \mathbf{n}_1 \\ \mathbf{n}_2 \\ \vdots \\ \mathbf{n}_j \end{bmatrix}, \tag{19}$$

where we set $\sqrt{\gamma}_k = 1$ without loss of generality. In order to eliminate the interference term, we require that $\mathbf{H}_k \mathbf{W}_i = \mathbf{0}, \forall i \neq k$, where $\mathbf{0}$ denotes an all-zero matrix. This equation can be written as

$$\overline{\mathbf{H}}_k \mathbf{W}_k = \mathbf{0}, \quad k = 1, 2, \ldots, j, \tag{20}$$

where the matrix $\overline{\mathbf{H}}_k$ contains all user's matrices in the system except that of the k-th user, i.e.,

$$\overline{\mathbf{H}}_k = \left[(\mathbf{H}_1)^H, \ldots, (\mathbf{H}_{k-1})^H, (\mathbf{H}_{k+1})^H, \ldots, (\mathbf{H}_K)^H \right]^H. \tag{21}$$

The matrix $\mathbf{W}_k$ can be obtained by decomposing $\overline{\mathbf{H}}_k$ into its singular values as

$$\overline{\mathbf{H}}_k = \mathbf{U}_k[\mathbf{\Sigma}_k, \mathbf{0}]\left[\mathbf{V}_k^{(1)}\mathbf{V}_k^{(0)}\right]^H, \tag{22}$$

where $\mathbf{U}_k$ is a unitary matrix, $\mathbf{\Sigma}_k$ is a diagonal matrix containing the non-negative singular values of $\overline{\mathbf{H}}_k$ with dimension equals to the rank of $\overline{\mathbf{H}}_k$, $\mathbf{0}$ is an all-zero matrix, $\mathbf{V}_k^{(1)}$ contains vectors corresponding to the nonzero singular values and $\mathbf{V}_k^{(0)}$ contains vectors corresponding to the zero singular values. The matrix $\mathbf{V}_k^{(0)}$ contains the last N_r columns of $\mathbf{V}_k$, which form an orthogonal basis that is in the null space of $\overline{\mathbf{H}}_k$. Then, $\mathbf{V}_k^{(0)}$ can be used as the precoding matrix $\mathbf{W}_k$ in Precoder 1. Note that the BD technique is applied for $N_t = jN_r$, where j is the number of users under MUI. Considering (20), the received signal is reduced to

$$\mathbf{y}_k = \mathbf{H}_k\mathbf{W}_k\tilde{\mathbf{x}}_k + \mathbf{n}_k, \tag{23}$$

which is an interference-free signal. Finally, the complete system is reduced to

$$\begin{bmatrix}\mathbf{y}_1\\ \mathbf{y}_2\\ \vdots\\ \mathbf{y}_j\end{bmatrix} = \begin{bmatrix}\mathbf{H}_1\mathbf{W}_1 & \cdots & \mathbf{0}\\ \mathbf{0} & \cdots & \mathbf{0}\\ \vdots & \ddots & \vdots\\ \mathbf{0} & \cdots & \mathbf{H}_j\mathbf{W}_j\end{bmatrix}\begin{bmatrix}\tilde{\mathbf{x}}_1^1\\ \tilde{\mathbf{x}}_1^2\\ \vdots\\ \tilde{\mathbf{x}}_1^j\end{bmatrix} + \begin{bmatrix}\mathbf{n}_1\\ \mathbf{n}_2\\ \vdots\\ \mathbf{n}_j\end{bmatrix}, \tag{24}$$

which shows the cancellation of the undesired components in the destination.

4.2. Strategy II. Joint-BD Precoding

In order to improve the flexibility in the design of the systems with $N_s \geq N_t$, a joint-precoding strategy is proposed in this subsection. Strategy II combines the channel matrix $\mathbf{G}$ and all channel matrices $\mathbf{H}_k$ in order to generate an equivalent channel matrix for each user. Then, the BD technique can be used to precancel the interference in both hops at the same time. Figure 5 shows a block diagram of the strategy II utilized.

Strategy II can be used when all users are under MUI or when all users see the complete RIS. Let us consider an equivalent matrix defined as $\mathbf{H}_k^{Eq} \triangleq (\mathbf{H}_k\mathbf{\Theta}\mathbf{G}) \in \mathbb{C}^{N_r \times N_t}$. Then, the received signal for the k-th user in (10) can be rewritten as

$$\mathbf{y}_k = \sqrt{\gamma}_k\mathbf{H}_k^{Eq}\mathbf{t}_\mathbf{x} + \mathbf{n}_k, \tag{25}$$

Considering $\mathbf{P} = \mathbf{I}$ in the Precoder 2, it follows that $\mathbf{t}_\mathbf{x} = \mathbf{x}$. Now, considering a precoding matrix $\mathbf{Z}_k^{Eq} \in \mathbb{C}^{N_t \times N_r}$ for the k-th user, the transmission vector in Precoder 1 can be written as

$$\mathbf{t}_\mathbf{x} = \sum_{k=1}^{K}\mathbf{Z}_k^{Eq}\tilde{\mathbf{x}}_k. \tag{26}$$

The received signal by the k-th user can be written as

$$\mathbf{y}_k = \sqrt{\gamma}_k\mathbf{H}_k^{Eq}\sum_{k=1}^{K}\mathbf{Z}_k^{Eq}\tilde{\mathbf{x}}_k + \mathbf{n}_k, \tag{27}$$

which can be also expressed as

$$\mathbf{y}_k = \sqrt{\gamma}_k\mathbf{H}_k^{Eq}\mathbf{Z}_k^{Eq}\tilde{\mathbf{x}}_k + \sqrt{\gamma}_k\mathbf{H}_k^{Eq}\sum_{i=1,i\neq k}^{K}\mathbf{Z}_i^{Eq}\tilde{\mathbf{x}}_i + \mathbf{n}_k, \tag{28}$$

where the first term in (28) is the signal sent to the k-th user, the second term is the interference produced by the other users in the system, whereas the third term is the noise. In order to remove the interference term, we require that $\mathbf{H}_k^{Eq}\mathbf{Z}_i^{Eq} = \mathbf{0}, \forall i \neq k$.

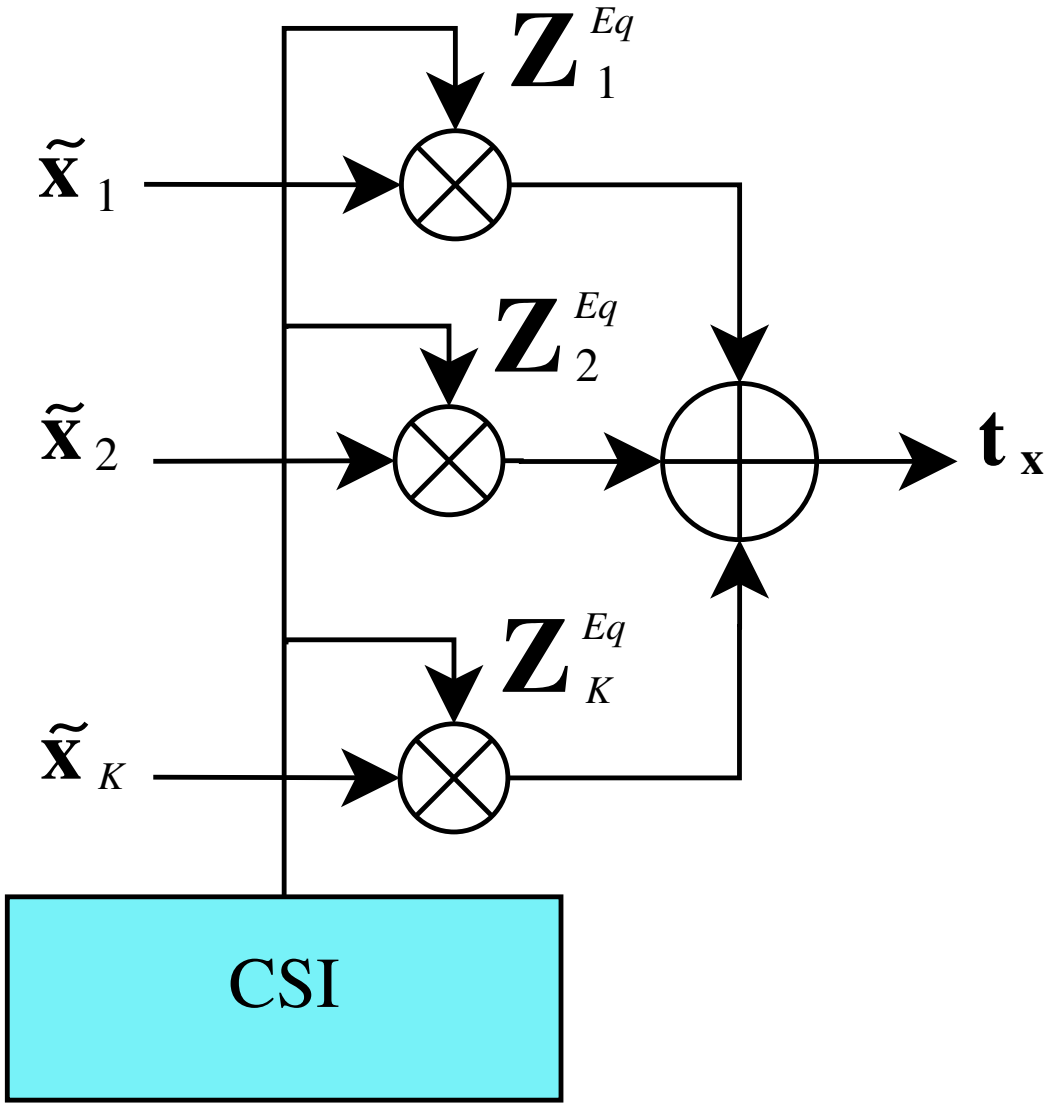

Figure 5. Strategy II (joint-BD precoder).

This condition can be written as

$$\overline{\mathbf{H}}_k^{Eq}\mathbf{Z}_k^{Eq} = \mathbf{0}, \quad k = 1, 2, \ldots, K, \tag{29}$$

where the matrix $\overline{\mathbf{H}}_k^{Eq}$ contains all users matrices in the system except that of the k-th user, i.e.,

$$\overline{\mathbf{H}}_k^{Eq} = \left[(\mathbf{H}_1^{Eq})^H, \ldots, (\mathbf{H}_{k-1}^{Eq})^H, (\mathbf{H}_{k+1}^{Eq})^H, \ldots, (\mathbf{H}_K^{Eq})^H\right]^H. \tag{30}$$

The matrix $\mathbf{Z}_k^{Eq}$ is obtained by decomposing $\overline{\mathbf{H}}_k^{Eq}$ into its singular values as

$$\overline{\mathbf{H}}_k^{Eq} = \mathbf{U}_k[\mathbf{\Sigma}_k, \mathbf{0}]\left[\mathbf{V}_k^{(1)}\mathbf{V}_k^{(0)}\right]^H. \tag{31}$$

Similar to (22), $\mathbf{\Sigma}_k$ is a diagonal matrix containing the non-negative singular values of $\overline{\mathbf{H}}_k^{Eq}$ and the matrix $\mathbf{V}_k^{(0)}$ contains the last N_r columns of $\mathbf{V}_k$, which form an orthogonal basis that is in the null space of $\overline{\mathbf{H}}_k^{Eq}$. Eliminating the interference term in (28), the received signal can be rewritten as

$$\mathbf{y}_k = \sqrt{\gamma_k}\mathbf{H}_k^{Eq}\mathbf{Z}_k^{Eq}\tilde{\mathbf{x}}_k + \mathbf{n}_k, \tag{32}$$

which is an interference-free signal. Finally, the complete system can be represented as

$$\begin{bmatrix} \mathbf{y}_1 \\ \mathbf{y}_2 \\ \vdots \\ \mathbf{y}_K \end{bmatrix} = \begin{bmatrix} \mathbf{H}_1^{Eq}\mathbf{Z}_1^{Eq} & \cdots & \mathbf{0} \\ \mathbf{0} & \cdots & \mathbf{0} \\ \vdots & \ddots & \vdots \\ \mathbf{0} & \cdots & \mathbf{H}_K^{Eq}\mathbf{Z}_K^{Eq} \end{bmatrix} \begin{bmatrix} \tilde{\mathbf{x}}_1 \\ \tilde{\mathbf{x}}_2 \\ \vdots \\ \tilde{\mathbf{x}}_K \end{bmatrix} + \begin{bmatrix} \mathbf{n}_1 \\ \mathbf{n}_2 \\ \vdots \\ \mathbf{n}_K \end{bmatrix}. \tag{33}$$

where $\sqrt{\gamma_k} = 1$ without loss of generality. Note that, differently from Strategy I, the precoding matrix $\mathbf{Z}_k^{Eq}$ can be used for arbitrary values of N_s. From here on, the systems based on Strategy I and Strategy II shall be referred to as RIS-MU-DQSM-I and RIS-MU-DQSM-II, respectively.

5. Detection

Assuming that the receiver has perfect knowledge of the channel gains, the maximum likelihood (ML) criterion compares the Euclidean distance between the received signal and all possible noiseless received signals in the system. The optimal ML detection criterion for the RIS-MU-DQSM-I system is defined as

$$\hat{\tilde{\mathbf{x}}}_k = \underset{\tilde{x}\in\mathcal{A}}{\operatorname{argmin}} \parallel \mathbf{y}_k - \mathbf{H}_k\mathbf{W}_k\mathbf{D} \parallel_F^2 . \tag{34}$$

where the matrix $\mathbf{D} \in \mathbb{C}^{Nr\times 2^m}$ accounts for the complete group of possible noiseless DQSM signals in the reception. For those users who are free of MUI, $\mathbf{W}_k = \mathbf{I}$ in (34). For the RIS-MU-DQSM-II system, the ML detection criterion is defined as

$$\hat{\tilde{\mathbf{x}}}_k = \underset{\tilde{\mathbf{x}}\in\mathcal{A}}{\operatorname{argmin}} \parallel \mathbf{y}_k - \mathbf{H}_k\mathbf{G}\mathbf{Z}_k^{Eq}\mathbf{D} \parallel_F^2 . \tag{35}$$

Detection Complexity

The detection complexity (η) of the analyzed systems is evaluated by counting the total number of floating-point operations (flops) required for the detection. All systems are compared considering the optimal ML detection criterion. For real additions, multiplications, and comparisons, 1 flop is carried out. For complex additions and multiplications, 2 and 6 flops are carried out, respectively, while subtractions and divisions take the same number as additions and multiplications respectively. Multiplication of $m \times n$ and $n \times p$ complex matrices uses $8mnp$ flops. Obtaining $\mathbf{Q}_k = \mathbf{H}_k\mathbf{W}_k$ in (34) requires $8N_r^2N_s$ flops. In order to obtain the noiseless version of the received signal in (34), we multiply $\mathbf{Q}_k \in \mathbb{C}^{Nr\times Nr}$ by the matrix $\mathbf{D} \in \mathbb{C}^{Nr\times 2^m}$, which represent all Rx antennas for the user k. This multiplication requires $8N_r^2 2^m\xi$ flops. For DQSM, when some spatial symbols are set to zero, the real size of the spatial constellation is reduced in the same proportion. The factor ξ is introduced to take into account the reduction of the size of the spatial constellation in comparison to the conventional QAM constellations. This factor is obtained by counting the number of zero-value inputs in the DQSM constellation.

$$\xi = 1 - \frac{zero\ entries}{2^m}. \tag{36}$$

Subtraction in the ML criterion requires $2N_r2^m$ flops, obtaining the absolute values requires $3N_r2^m$ flops, the maximum ratio combining (MRC) for the received signals of each Rx antenna requires $2N_r2^m$ flops, and ordering all results to find the minimum requires $2(2^m)$ flops. Adding the last four partial results, we obtain $7N_r2^m\xi$ flops approximately. Table 2 summarizes the complexity of partial operation carried out for Strategy I and Strategy II.

Table 2. Detection complexity.

Operation	Complexity
$\mathbf{Q}_k = \mathbf{H}_k\mathbf{W}_k$	$8N_r^2N_s$
$\mathbf{Q}_k\mathbf{D}$	$8N_r^2 2^m \xi$
Subtractions	$2N_r 2^m$
$\|\cdot\|_F^2$	$3N_r 2^m$
MRC	$2N_r 2^m$
Ordering	$2(2^m)$
$\mathbf{Q} = \mathbf{H}_k\mathbf{G}$	$8N_rN_sN_t$
$\mathbf{P} = \mathbf{Q}\mathbf{Z}_k^{Eq}$	$8N_r^2N_t$
$\mathbf{PD}$	$8N_r^2 2^m \xi$

Finally, adding all these partial results, the detection complexity for the RIS-MU-DQSM-I system is

$$\eta_I \approx 8N_r^2N_s + 8N_r^2 2^m \xi + 7N_r 2^m \xi. \tag{37}$$

The detection complexity for the RIS-MU-DQSM-II system (35) is obtained as follows: The product of $\mathbf{H}_k \in \mathbb{C}^{Nr \times Ns}$ by $\mathbf{G} \in \mathbb{C}^{Ns \times Nt}$ requires $8N_rN_sN_t$ flops. Multiplying by the matrix $\mathbf{Z}_k^{Eq} \in \mathbb{C}^{N_t \times N_r}$ requires $8N_r^2N_t$ flops. Multiplying by matrix $\mathbf{D} \in \mathbb{C}^{Nr \times 2^m}$ requires $8N_r^2 2^m \xi$. Similar to (37), ML criterion requires $7N_r^2 2^m \xi$ flops approximately. Adding all these partial results, we obtain the detection complexity for Strategy II as

$$\eta_{II} \approx 8N_rN_sN_t + 8N_r^2N_t + 8N_r^2 2^m \xi + 7N_r 2^m \xi. \tag{38}$$

In (37) and (38), ξ takes into account that the lattice of the DQSM constellation is reduced by the inserted zeros [19]. Then, for the conventional MU-MIMO-SMux system $\xi = 1$. For the RIS-MU-DQSM schemes, the factor ξ is evaluated by directly counting the entries with zero value in the real or imaginary parts of the spatial constellation. Considering a SE of 8 bits per channel use (bpcu)/user, we obtain $\xi = 0.75$, meanwhile for an SE of 12 bpcu/user $\xi = 0.4375$. In the next section, the results of complexity are analyzed and discussed.

6. Results and Discussion

In this section, we analyze and discuss the BER performance and the detection complexity of the proposed system considering two configurations with different SE and two different scenarios: the uncorrelated and the correlated channels. The results of the proposed system are compared with the conventional MU-MIMO-SMux system [22] and with the recently proposed relay-assisted AF-MU-DQSM system [23] under the same conditions and parameters.

6.1. Detection Complexity Results

In order to obtain fair comparisons, all systems are using optimal ML detection criterion. Table 3 shows a comparison of the detection complexity for all systems considering the two configurations used as study cases. The results show that considering the $(4 \times 2) \times 8 \times 8$ configuration with an SE of 8 bpcu, the RIS-MU-DQSM-I, and the RIS-MU-DQSM-II systems have 25% and 16% lower detection complexity, respectively, when compared with the conventional MU-MIMO-SMux scheme. Considering the $(8 \times 4) \times 32 \times 32$ configuration with an SE of 12 bpcu, the proposed RIS-MU-DQSM-I and the RIS-MU-DQSM-II systems have 56% and 51% lower detection complexity, respectively, when compared with the conventional MU-MIMO-SMux system used as reference. The AF-MU-DQSM system used as a second reference has the same detection complexity as the RIS-MU-DQSM-II system since they are using the same modulation, precoding, and detection strategies.

Table 3. Detection complexity.

System Configuration	RIS-MU DQSM-I	RIS-MU DQSM-II	AF-MU DQSM	MU-MIMO SMux
$(4 \times 2) \times 8 \times 8$ $(4 \times 2) \times 8$	9088	10,112	10,112	12,032
$(8 \times 4) \times 32 \times 32$ $(8 \times 4) \times 32$	283,648	316,416	316,416	643,072

All systems are evaluated for the optimal ML detection criterion.

6.2. BER Performance

For simulations, all systems are using a normalized transmission energy per user, i.e., $\mathbb{E}[\| \mathbf{t_x}^H \mathbf{t_x} \|] = K$, the same number of Tx/Rx antennas, and the same SE. Also, all systems are using similar precoding strategies and the optimal ML detection criterion alike. In order to carry out fair comparisons, all systems are compared considering MUI. The channel uses a spatial correlation coefficient of $\rho = 0.7$ in the BS and the RIS/relays. Tables 4 and 5 show the configuration and the QAM constellation utilized for SE = 8 bpcu/user and SE = 12 bpcu/user, respectively. Note that systems using spatial modulation require lower-order QAM constellations, while the conventional system requires higher-order QAM constellations to achieve the desired SE. All simulations were carried out using MATLAB SA 2015®.

Table 4. Simulation parameters for SE = 8 bpcu/user, 4 users, $N_t = 8$, $N_r = 2$, L = 2.

Scheme	Configuration	QAM Mod.
RIS-MU-DQSM-I	$(4 \times 2) \times 8 \times 8$	4-QAM
RIS-MU-DQSM-II	$(4 \times 2) \times 8 \times 8$ $(4 \times 2) \times 16 \times 8$ $(4 \times 2) \times 32 \times 8$	4-QAM
AF-MU-DQSM	$(4 \times 2) \times 8 \times 8$ $(4 \times 2) \times 16 \times 8$ $(4 \times 2) \times 32 \times 8$	4-QAM
MU-MIMO-SMux	$(4 \times 2) \times 8$	8-QAM

Table 5. Simulation parameters for SE = 12 bpcu/user, 8 users, $N_t = 32$, $N_r = 4$, L = 4.

Scheme	Configuration	QAM Mod.
RIS-MU-DQSM-I	$(8 \times 4) \times 32 \times 32$	4-QAM
RIS-MU-DQSM-II	$(8 \times 4) \times 32 \times 32$ $(8 \times 4) \times 48 \times 32$ $(8 \times 4) \times 64 \times 32$	4-QAM
AF-MU-DQSM	$(8 \times 4) \times 32 \times 32$ $(8 \times 4) \times 48 \times 32$ $(8 \times 4) \times 64 \times 32$	4-QAM
MU-MIMO-SMux	$(8 \times 4) \times 32$	8-QAM

For the uncorrelated fading channel, and the $(4 \times 2) \times 32 \times 8$ configuration, the proposed RIS-MU-DQSM-II system has 17 dB and 15 dB BER performance gains when compared with the conventional MU-MIMO-SMux and the AF-MU-DQSM systems, respectively, as shown in Figure 6. For the $(8 \times 4) \times 64 \times 32$ configuration, the proposed RIS-MU-DQSM-II system has 14 dB and 18 dB BER performance gains when compared with the conventional MU-MIMO-SMux and the AF-MU-DQSM systems, respectively, as shown in Figure 7.

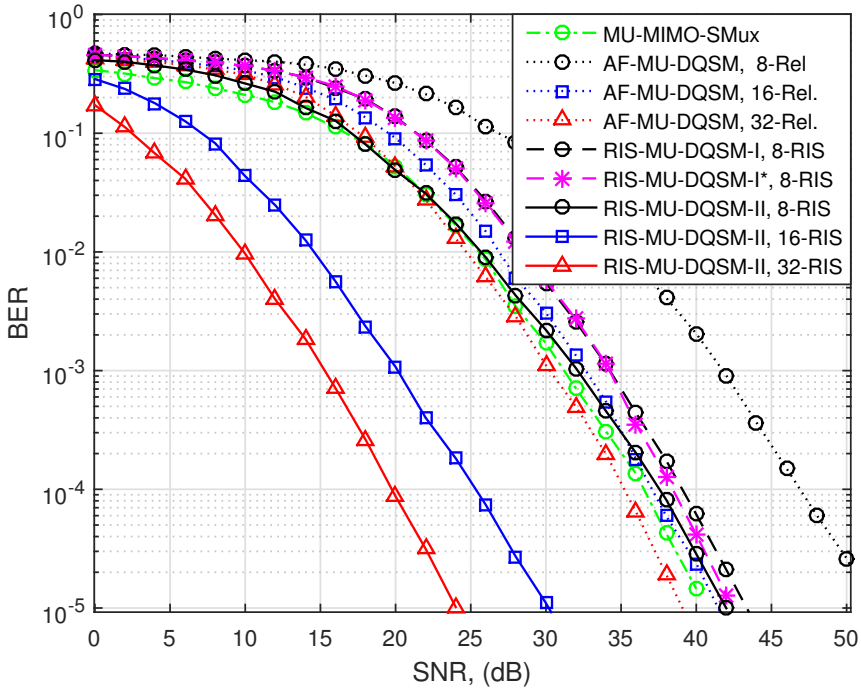

Figure 6. BER Performance comparison for a SE of 8 bpcu/user, L = 2, 4 users, and the uncorrelated fading channel.

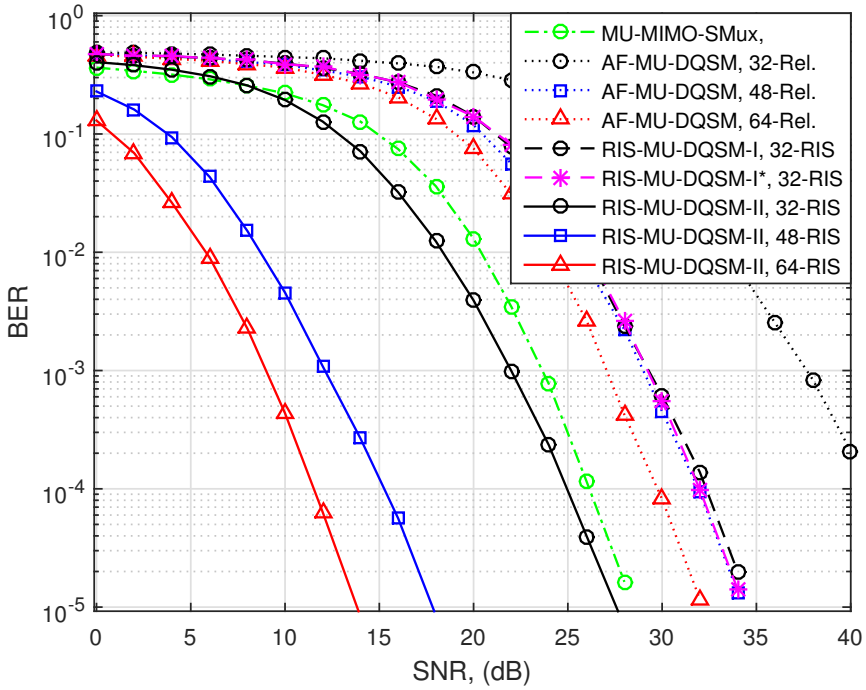

Figure 7. BER performance comparison for a SE of 12 bpcu/user, L = 4, 8 users, and the uncorrelated fading channel.

As shown in Figures 8 and 9, when the correlated fading channel is considered, the RIS-MU-DQSM-II and the AF-MU-DQSM schemes are affected by 7 dB to 15 dB approximately. Under this scenario, the conventional MU-MIMO-Smux system is affected only by 5 dB. This result can be explained by the reflecting mirrors or the relaying antennas affected by the spatial correlation. On the other hand, the proposed RIS-MU-DQSM-I was only affected by 2–3 dB. It means that the ZF technique is robust under the correlated fading scenario. Note that users who are free of MUI (marked as RIS-MU-DQSM-I*) have a similar

BER performance that the other users under MUI. This fact shows the robustness of the BD technique used to avoid interference in the second hop. It is worth noting that when the proposed schemes are using a reduced number of mirrors in the RIS they have similar BER performance than the conventional MU-MIMO-SMux scheme. However, when an increased number of mirrors are used, the proposed RIS-MU-DQSM-II, clearly outperforms both schemes used as reference.

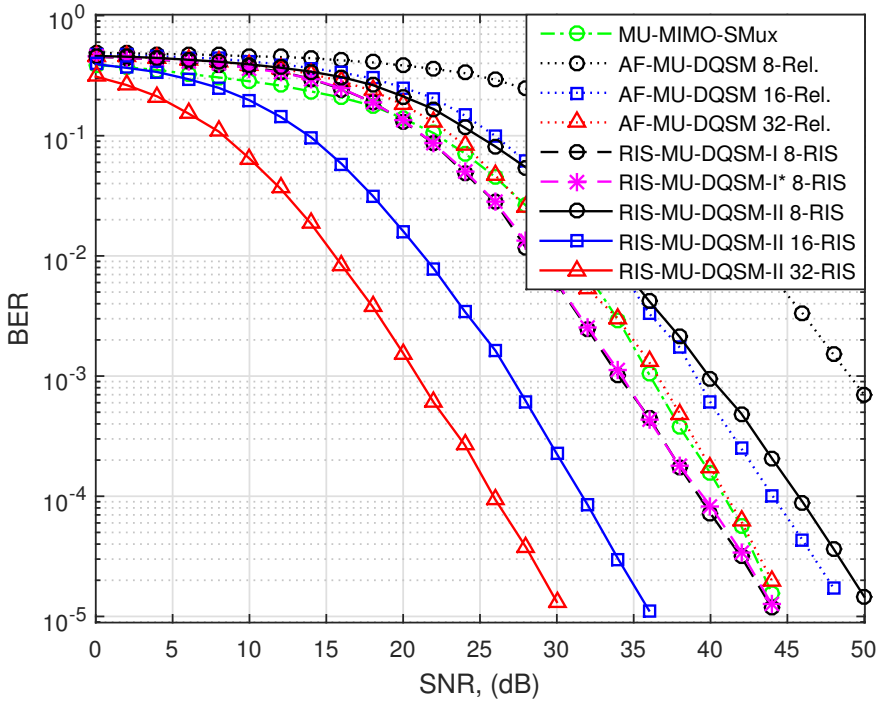

Figure 8. BER performance comparison for a SE of 8 bpcu/user, L = 2, 4 users, and a correlation factor of $\rho = 0.7$.

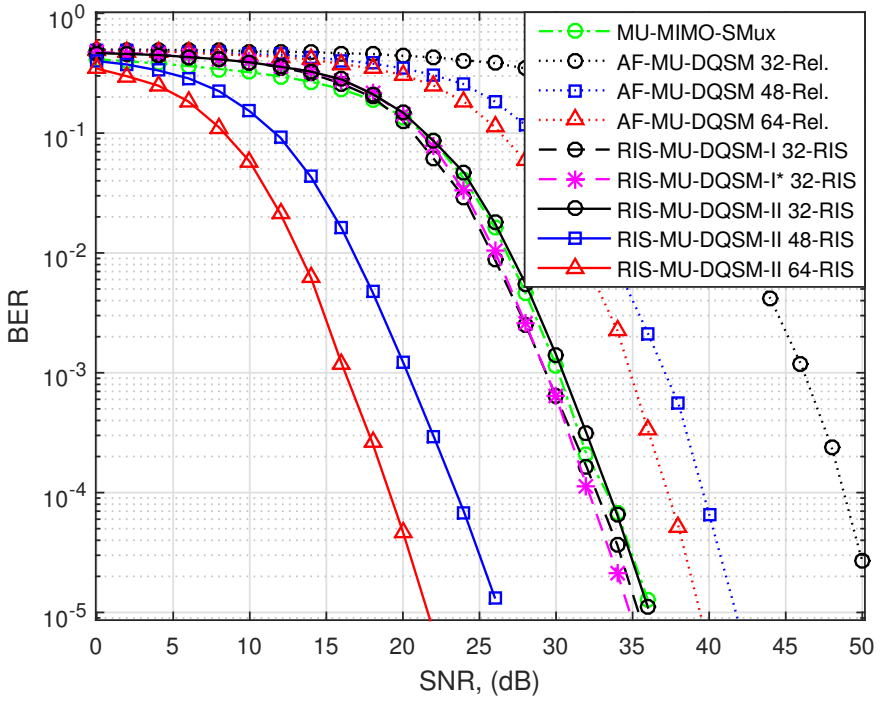

Figure 9. BER performance comparison for a SE of 12 bpcu/user, L = 4, 8 users, and a correlation factor of $\rho = 0.7$.

6.3. Discussion

RIS-based systems have strongly attracted attention since they improve the performance of the systems by optimizing the use of radiated energy. However, one drawback of the RIS-based system is the control of phases and amplitudes of the impinging signals in the RIS. Typically, an additional control unit in the RIS is required. However, this approach can be a challenge mainly when the RIS is located far from the transmitter or BS. Recently, RIS-assisted systems using spatial modulation have been considered as potential candidates for future 6G wireless communication systems [20,21,34]. However, previous works in this area are focused mainly on users with single Rx antenna (MISO) systems. The results obtained in this work show that the proposed system can effectively be used to pre-modify the amplitude and phases of the signals reflected by the RIS. This fact is important since in this case the signal processing required in the RIS is transferred to the BS where the hardware and software capabilities of the system make signal processing more adequate. Additionally, the utilized DQSM transmission scheme improves the overall performance and reduces the detection complexity of the system. Comparing the two proposed schemes, the RIS-MU-DQSM-I scheme has the lowest detection complexity. However, this scheme requires that $N_s = N_r$ for perfect interference cancellation. This limitation is overcome by the proposed RIS-MU-DQSM-II scheme, which also outperforms by 2 dB and 6 dB in BER the RIS-MU-DQSM-I scheme for the same SE of 8 bpcu/user and 12 bpcu/user, respectively. It is worth noting that in comparison with the conventional MU-MIMO-SMux systems, the RIS degrades the BER performance of the system when a limited number of mirrors is used. However, when N_s is greater than N_t, the RIS-based system takes advantage of diversity and significantly improves in BER.

As expected, the proposed system clearly outperforms the previous AF-MU-DQSM scheme. This fact is mainly due to the total quantity of noise in the RIS-based systems compared with the relay-assisted scheme used as a reference. However, it is fair to mention that relay-based systems can offer an extended coverage range compared with RIS. Considering the correlated channel scenario, both systems using a relay or RIS result were significantly affected compared with the conventional one. This fact highlights the need for RIS-based systems with low spatial correlation. Although the proposed system transfers any signal processing over the impinging signals in the RIS to the BS, the RIS is still responsible to change the reflecting angles of the reflecting mirrors. For this reason, the RIS still requires a low-speed reverse channel to track the MSs in the network and share the CSI. However, the manner in which the RIS carries out this task is beyond the scope of this paper. The proposed system reduces the required signal processing in the RIS, which is only responsible for tracking the mobile user in the network. This characteristic makes the proposed system suitable for the implementation of RIS-assisted 5G/6G systems. However, in order to improve the system proposed here, it would be desirable to integrate other techniques that can further improve the system's performance. For example, considering orthogonal frequency division multiplexing (OFDM) systems, the proposed technique could be improved in its spectral efficiency and system capacity. On the other hand, incorporating techniques such as non-orthogonal multiple access (NOMA) could result in a system with the ability to overcome the challenges of the wireless environment like random fluctuations, shadowing, and mobility in an energy-efficient way [35].

7. Conclusions

In this paper, two precoding techniques for a novel RIS-MU-DQSM downlink transmission system have been presented. Instead of being applied at the remote RIS, the phase shift vector is designed and applied at the BS, simplifying the system's design and implementation. Two different strategies were proposed and evaluated for the implementation of the proposed system. In the reception, the detection complexity of the system was improved 51% by incorporating a novel spatial modulation technique. Results show that the proposed RIS-MU-DQSM-I strategy has the lowest detection complexity. However, in this case, the ZF precoding imposes the condition $N_t = N_s$. This limitation was overcome

by the RIS-MU-DQSM-II strategy, which exploits the diversity in the RIS to obtain up to 18 dB gains in BER performance when compared with the conventional MU-MIMO-SMux system based on QAM and a similar based on AF relay under the same condition and parameters. Mainly, the proposed RIS-MU-DQSM system reduces the signal processing required at the remote RIS, making it suitable for practical implementations of future wireless communication networks.

Author Contributions: Conceptualization, F.R.C.-S. and C.A.A.-M.; methodology, J.A.D.P.-F., F.R.C.-S. and C.A.G.; software, J.S.; validation, J.S., F.R.C.-S. and V.B.K.; formal analysis, F.R.C.-S. and V.B.K.; investigation, F.R.C.-S., C.A.A.-M., J.S., C.A.G. and J.A.D.P.-F.; resources, J.A.D.P.-F., F.R.C.-S. and C.A.G.; writing, original draft preparation, F.R.C.-S.; writing, review and editing, C.A.A.-M., V.B.K., J.S. and C.A.G.; supervision, V.B.K.; project administration, J.A.D.P.-F. and F.R.C.-S.; funding acquisition, J.A.D.P.-F. All authors read and agreed to the published version of the manuscript.

Funding: The authors would like to thank Universidad Panamericana, for their support through the program "Fomento a la Investigación UP 2022", and the project "Diseño de sistema de comunicación vehículo a vehículo MIMO-OFDM basado en modulación por índice" UP-CI-2022-GDL-ING, and to the Universidad Panamericana Dirección Institucional de Investigación. The Proyects FONDECYT Regular 1211132, and STIC-AmSud AMSUD220026.

Data Availability Statement: Not applicable.

Conflicts of Interest: The authors declare no conflict of interest.

References

1. Huo, Y.; Lin, X.; Di, B.; Zhang, H.; Hernando, F.J.L.; Tan, A.S.; Mumtaz, S.; Demir, Ö.T.; Chen-Hu, K. Technology Trends for Massive MIMO towards 6G. *Sensors* **2023**, *23*, 6062. [CrossRef]
2. Pérez-Adán, D.; Fresnedo, Ó.; González-Coma, J.P.; Castedo, L. Intelligent Reflective Surfaces for Wireless Networks: An Overview of Applications, Approached Issues, and Open Problems. *Electronics* **2021**, *10*, 2345. [CrossRef]
3. He, X.; Cui, Y.; Tentzeris, M. Tile-based massively scalable MIMO and phased arrays for 5G/B5G-enabled smart skins and reconfigurable intelligent surfaces. *Sci. Rep.* **2022**, *12*, 2741. [CrossRef]
4. Wang, Y.; Zhang, W.; Chen, Y.; Wang, C.X.; Sun, J. Novel Multiple RIS-Assisted Communications for 6G Networks. *IEEE Commun. Lett.* **2022**, *26*, 1413–1417. [CrossRef]
5. Tang, W.; Chen, M.Z.; Chen, X.; Dai, J.Y.; Han, Y.; Di Renzo, M.; Zeng, Y.; Jin, S.; Cheng, Q.; Cui, T.J. Wireless Communications With Reconfigurable Intelligent Surface: Path Loss Modeling and Experimental Measurement. *IEEE Trans. Wirel. Commun.* **2021**, *20*, 421–439. [CrossRef]
6. Basar, E.; Di Renzo, M.; De Rosny, J.; Debbah, M.; Alouini, M.S.; Zhang, R. Wireless Communications Through Reconfigurable Intelligent Surfaces. *IEEE Access* **2019**, *7*, 116753–116773. [CrossRef]
7. Malathy, S.; Jayarajan, P.; Ojukwu, H.; Qamar, F.; Hindia, M.H.D.N.; Dimyati, K.; Noordin, K.A.; Amiri, I.S. A review on energy management issues for future 5G and beyond network. *Wirel. Netw.* **2021**, *27*, 2691–2718. [CrossRef]
8. Alanazi, F. Intelligent reflecting surfaces with energy harvesting for Nakagami fading channels. *Telecommun. Syst.* **2021**, *78*, 351–361. [CrossRef]
9. Alamzadeh, I.; Alexandropoulos, G.; Shlezinger, N.; Imani, M.F. A reconfigurable intelligent surface with integrated sensing capability. *Sci. Rep.* **2021**, *11*, 20737. [CrossRef] [PubMed]
10. Zhang, H.; Di, B. Intelligent Omni-Surfaces: Simultaneous Refraction and Reflection for Full-Dimensional Wireless Communications. *IEEE Commun. Surv. Tutor.* **2022**, *24*, 1997–2028. [CrossRef]
11. Bansal, A.; Agrawal, N.; Singh, K.; Li, C.P. RIS Selection Scheme for UAV-based Multi-RIS-aided Multiuser Downlink Network with Imperfect and Outdated CSI. *IEEE Trans. Commun.* **2023**, *71*, 4650–4664. [CrossRef]
12. Zargari, S.; Khalili, A.; Zhang, R. Energy Efficiency Maximization via Joint Active and Passive Beamforming Design for Multiuser MISO IRS-Aided SWIPT. *IEEE Wirel. Commun. Lett.* **2021**, *10*, 557–561. [CrossRef]
13. Wang, X.; Fei, Z.; Guo, J.; Zheng, Z.; Li, B. RIS-Assisted Spectrum Sharing Between MIMO Radar and MU-MISO Communication Systems. *IEEE Wirel. Commun. Lett.* **2021**, *10*, 594–598. [CrossRef]
14. Papazafeiropoulos, A.K.; Pan, C.; Kourtessis, P.; Chatzinotas, S.; Senior, J.M. Intelligent Reflecting Surface-assisted MU-MISO Systems with Imperfect Hardware: Channel Estimation, Beamforming Design. *arXiv* **2021**, arXiv:2102.05333.
15. Huang, C.; Mo, R.; Yuen, C. Reconfigurable Intelligent Surface Assisted Multiuser MISO Systems Exploiting Deep Reinforcement Learning. *IEEE J. Sel. Areas Commun.* **2020**, *38*, 1839–1850. [CrossRef]
16. Souto, N.; Silva, J.C. Joint Beamforming Algorithm for Multi-stream MIMO Systems Assisted by Multiple Reconfigurable Intelligent Surfaces. *IEEE Open J. Commun. Soc.* **2023**, *4*, 1317–1333. [CrossRef]

17. Semmler, D.; Joham, M.; Utschick, W. Linear Precoding in the Intelligent Reflecting Surface Assisted MIMO Broadcast Channel. In Proceedings of the 2022 IEEE 23rd International Workshop on Signal Processing Advances in Wireless Communication (SPAWC), Oulu, Finland, 4–6 July 2022; pp. 1–5. [CrossRef]
18. Cai, S.; Qu, H.; Zhang, J.; Shi, X.; Zhu, H. Symbol-Level Precoding Design in IRS-Aided Secure Wireless Communication Systems. *IEEE Wirel. Commun. Lett.* **2022**, *11*, 2315–2319. [CrossRef]
19. Castillo-Soria, F.; Cortez, J.; Gutiérrez, C.; Luna-Rivera, M.; Garcia-Barrientos, A. Extended quadrature spatial modulation for MIMO wireless communications. *Phys. Commun.* **2019**, *32*, 88–95. [CrossRef]
20. Basar, E. Reconfigurable Intelligent Surface-Based Index Modulation: A New Beyond MIMO Paradigm for 6G. *IEEE Trans. Commun.* **2020**, *68*, 3187–3196. [CrossRef]
21. Bamisaye, A.J.; Quazi, T. Quadrature spatial modulation-aided single-input multiple-output-media-based modulation. *Int. J. Commun. Syst.* **2021**, *34*, e4883. [CrossRef]
22. Khan, M.H.A., Chung, J.; Lee, M. Lattice reduction aided with block diagonalization for multiuser MIMO systems. *J. Wirel. Commun. Netw.* **2015**, *2015*, 254. [CrossRef]
23. Castillo-Soria, F. AF relay assisted multiuser MIMO-DQSM downlink transmission system. *Electron. Lett.* **2020**, *56*, 682–684. [CrossRef]
24. Nadeem, Q.U.A.; Kammoun, A.; Chaaban, A.; Debbah, M.; Alouini, M.S. Asymptotic Max-Min SINR Analysis of Reconfigurable Intelligent Surface Assisted MISO Systems. *IEEE Trans. Wirel. Commun.* **2020**, *19*, 7748–7764. [CrossRef]
25. Huang, C.; Zappone, A.; Alexandropoulos, G.C.; Debbah, M.; Yuen, C. Reconfigurable Intelligent Surfaces for Energy Efficiency in Wireless Communication. *IEEE Trans. Wirel. Commun.* **2019**, *18*, 4157–4170. [CrossRef]
26. Mohades, Z.; Tabataba, V.V. Deep Neural Network for Compressive Sensing and Application to Massive MIMO Channel Estimation. *Circuits Syst. Signal Process.* **2021**, *40*, 4474–4489. [CrossRef]
27. Rao, X.; Lau, V.K.N.; Kong, X. CSIT estimation and feedback for FDD multi-user massive MIMO systems. In Proceedings of the 2014 IEEE International Conference on Acoustics, Speech and Signal Processing (ICASSP), Florence, Italy, 4–9 May 2014; pp. 3157–3161. [CrossRef]
28. Han, Y.; Tang, W.; Jin, S.; Wen, C.K.; Ma, X. Large Intelligent Surface-Assisted Wireless Communication Exploiting Statistical CSI. *IEEE Trans. Veh. Technol.* **2019**, *68*, 8238–8242. [CrossRef]
29. Mesleh, R.; Ikki, S.S.; Aggoune, H.M. Quadrature Spatial Modulation. *IEEE Trans. Veh. Technol.* **2015**, *64*, 2738–2742. [CrossRef]
30. Martin, C.; Ottersten, B. Asymptotic eigenvalue distributions and capacity for MIMO channels under correlated fading. *IEEE Trans. Wirel. Commun.* **2004**, *3*, 1350–1359. [CrossRef]
31. Wiesel, A.; Eldar, Y.C.; Shamai, S. Zero-Forcing Precoding and Generalized Inverses. *IEEE Trans. Signal Process.* **2008**, *56*, 4409–4418. [CrossRef]
32. Raviv, L.o.; Leshem, A. Scheduling for Multi-User Multi-Input Multi-Output Wireless Networks with Priorities and Deadlines. *Future Internet* **2019**, *11*, 172. [CrossRef]
33. Spencer, Q.; Swindlehurst, A.; Haardt, M. Zero-forcing methods for downlink spatial multiplexing in multiuser MIMO channels. *IEEE Trans. Signal Process.* **2004**, *52*, 461–471. [CrossRef]
34. Li, Q.; Wen, M.; Wang, S.; Alexandropoulos, G.C.; Wu, Y.C. Space Shift Keying With Reconfigurable Intelligent Surfaces: Phase Configuration Designs and Performance Analysis. *IEEE Open J. Commun. Soc.* **2021**, *2*, 322–333. [CrossRef]
35. Kumaravelu, V.B.; Imoize, A.L.; Soria, F.R.C.; Velmurugan, P.G.S.; Thiruvengadam, S.J.; Do, D.T.; Murugadass, A. RIS-Assisted Fixed NOMA: Outage Probability Analysis and Transmit Power Optimization. *Future Internet* **2023**, *15*, 249. [CrossRef]